Optimization of bi-metallic (Fe–Co) catalyst on kaolin support for carbon nanofiber growth in a CVD reactor

K. Y. Mudi, A. S. Abdulkareem, O. S. Azeez, A. S. Kovo, J. O. Tijani & E. J. Eterigho

Carbon Letters

ISSN 1976-4251

Carbon Lett.
DOI 10.1007/s42823-019-00036-w

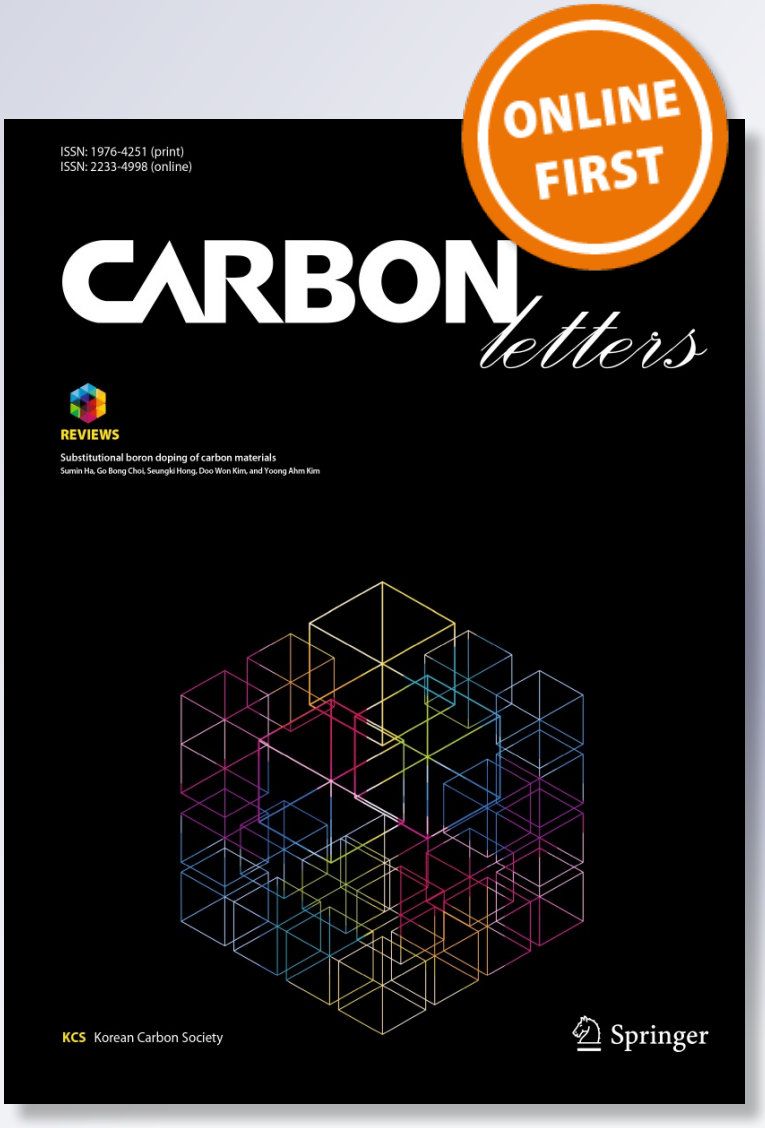

Springer

Carbon Letters
https://doi.org/10.1007/s42823-019-00036-w

Online ISSN 2233-4998
Print ISSN 1976-4251

ORIGINAL ARTICLE

Optimization of bi-metallic (Fe–Co) catalyst on kaolin support for carbon nanofiber growth in a CVD reactor

K. Y. Mudi[3,4] · A. S. Abdulkareem[1,4] · O. S. Azeez[1] · A. S. Kovo[1,4] · J. O. Tijani[2,4] · E. J. Eterigho[1]

Received: 16 May 2018 / Accepted: 20 June 2018

Abstract

This study focused on the development of Fe–Co/kaolin catalyst by a wet impregnation method. Response surface methodology was used to study the influence of operating variables such as drying temperature, drying time, mass of support and stirring speed on the yield of the catalyst. The catalyst composite at best synthesis conditions was then calcined in an oven at varied temperature and time using 2^2 factorial design of experiment. The catalyst with optimum surface area was then utilized to grow carbon nanofiber (CNF) in a chemical vapour deposition (CVD) reactor. Both the catalyst and CNF were characterized using high-resolution scanning electron microscopy, high-resolution transmission electron microscopy, thermogravimetric analysis (TGA), X-ray diffraction (XRD) and X-ray photoelectron spectroscopy. On the influence of operating variables on the yield of catalyst, the results showed that an optimum yield of 96.51% catalyst was obtained at the following operating conditions: drying time (10 h), drying temperature (110 °C), stirring speed (100 rpm) and mass of support (9 g). Statistical analysis revealed the existence of significant interactive effects of the variables on the yield of the catalyst. The HRSEM/XRD/BET/TGA analysis revealed that the particles are well dispersed on the support, with high surface area (376.5 m^2/g) and thermally stable (330.88 °C). The influence of operating parameters on the yield of CNF was also investigated and the results revealed an optimum yield of 348% CNF at the following operating conditions: reaction temperature (600 °C), reaction time (40 min), argon flow rate (1416 mL/min) and acetylene/hydrogen flow rate (1416 mL/min). It was found from statistical analysis that the reaction temperature and acetylene/hydrogen flow rates exerted significant effect on the CNF yield than the other factors. The contour and surface plots bi-factor interaction indicated functional relationship between the response and the experimental factors. The characterization results showed that the synthesized CNF is thermally stable, twisted and highly crystalline and contain surface functional groups. It can be inferred from the results of various analyses that the developed catalyst is suitable for CNF growth in a CVD reactor.

Keywords Bi-metallic catalyst · Carbon nanofiber · Optimization · Characterization · Chemical vapour deposition

1 Introduction

CNF synthesis dated back as far as 1890, when it was produced as carbon filament (a nuisance) that was formed during catalytic conversion of carbon-containing gas [1, 2]. Since then, there have been concerted efforts on CNFs due to their unique potentials as well as their chemical similarity to fullerenes and carbon nanotubes (CNT).CNF is defined as a fibrous carbon material with more than 90% carbon content with high tensile strength, thermal and electrical conductivity and reasonable mechanical stability and durability under various temperatures and pressure ranges in extreme environments [3–5]. In comparison to CNT, CNFs have received much less attention because CNT has better properties such as higher tensile strength, smaller dimensions and lower

✉ K. Y. Mudi
m.kehinde@kadunapolytechnic.edu.ng

1 Department of Chemical Engineering, Federal University of Technology, Minna, Nigeria

2 Department of Chemistry, Federal University of Technology, Minna, Nigeria

3 Department of Chemical Engineering, Kaduna Polytechnic, Kaduna, Nigeria

4 Nanotechnology Research Group, Centre for Genetic Engineering and Biotechnology, Federal University of Technology, Minna, Nigeria

Published online: 08 February 2019

density. However, CNFs are regarded as excellent alternative to CNTs due to the fact that the structure and angular arrangement of fibers in the matrix provide exposed edges that enhance chemical functionalization. Their production process can be easily transferable to industrial scale, and as a result, CNFs are about 2–3 times cheaper than CNTs [6]. In addition, CNFs can be used for research purposes to build knowledge that might be transferable than the more expensive CNTs. The ease of handling CNF make it preferable since it prevents the challenges arising from dispersion, processing and handling that are peculiar to CNT [6].

In the last couple of years, researchers have employed various techniques to synthesize CNF which include the vaporization of graphite from an arc discharge, laser ablation methods and catalytic decomposition of carbon-containing compounds gases [1, 7, 8]. Of all the aforementioned techniques, CVD method has been the preferred choice over other techniques for a large-scale production of CNFs because of its selectivity, flexibility, cost-effectiveness and it is technically simple [9, 10]. In addition, the synthesis parameters such as the reaction temperature, flowrate of the carbon source and the amount of catalyst used can be readily adjusted such that different types of CNFs could be obtained [11]. In CVD technique, CNFs were synthesized by the decomposition of carbon source (usually hydrocarbons or carbon monoxides) in a tubular quartz reactor placed in a furnace in the presence of suitable catalyst and inert gas.

Metal catalysts mainly used for CVD are transition metals such as iron, cobalt and nickel and their alloys. The choice of these noble metals and their alloy was reported to have the ability to bring about reduction and prevents deactivation process of some hydrocarbon reactions [12]. They also have the ability to improve metal support interaction thereby increase the catalyst activity [13]. These metal catalysts are either used alone or as an alloy to obtain a high yield of CNF. For instance, Manafi and Badiee [14] reported that cobalt used as a catalyst to lithium fluoride produced high yield of more than 70% CNF by CVD. Seongyop et al. [15] also reported a high yield of 43–57% of CNF in a CVD reactor at low temperature of 480 °C with the application of nickel-supported catalyst. In the same vain, the findings of van der Lee et al. [16] showed that 50% yield of CNF was obtained using SiO_2-supported Ni catalyst. CNF of excellent crystallinity and morphology were also grown using nickel and molybdenum catalysts as reported by Eunyi et al. [17]. The use of iron catalyst has produced high yield of 158.2% helical CNF of good aspect ratio and morphology.

High yield of CNF by these catalysts was obtained with the use of various support materials that are stable at high temperatures, possesses high surface area, very easy to handle, very easy to regenerate with low cost and hence influence the activity of the catalyst [12, 18]. Some of the researchers who employed different support materials for the growth of CNF in a CVD reactor include Mamun et al. [19] who reported that the use of powdered activated carbon (PAC) as a support to nickel in the synthesis of CNF in a CVD reactor aided the growth of CNF and the formed CNF could be applied for various uses. In addition, as reported by Prasantha et al. [20], silica used as an iron-supported catalyst produced CNF of good morphology and arrangement by providing good bonding between carbon and created a good dispersion of the carbon in a cement matrix material. The platelet morphology of CNF with a uniform orientation was produced when alumina was used as a support to nickel catalyst in a CVD reactor by decomposition of liquid organic waste from chemical and petrochemical industries to yield 22–23% acetylene that served as carbon source [21]. In addition, the same alumina was used as support to bimetallic (Ni–Cu) catalyst for the investigation of the relationship between microstructure changes of the catalyst and the morphology of graphitic CNF using acetylene as the carbon source [22]. Other support materials used for synthesis CNF of good structural arrangements, morphology and applied for various applications include: silica [20], Na_2CO_3 [23], NaCl [24], maghemite [25] and nickel alloy [26]. Previously, Miao et al. [27] demonstrated the production of carbon nanotubes and carbon nanospheres on kaolin-supported transition monometallic (Fe, Co, and Ni) catalysts by CCVD technique and obtained high-yield carbon spheres of controlled size at the temperature range of 750–850 °C and reaction time of 30 min. Similarly, Xu et al. [28] produced two different kinds of carbon nanostructures namely carbon nanotubes and carbon spheres from kaolin- and ceramic-supported cobalt catalysts, respectively, via CCVD method. The authors found that only carbon spheres with diameter of 500–1500 nm was formed from the kaolin-supported catalyst while a mixture of carbon nanotubes and carbon spheres were obtained using ceramic plate. The authors opined that substrate played an important role in the formation of either carbon nanotubes or carbon spheres. Comparatively, it can be noticed that the authors used monometallic catalyst for the synthesis of the nanomaterials and the synergetic effect which perhaps determined the quality and yields of carbon materials were not studied. Additionally, proper optimization of synthesis parameters using surface response methodology was not carried out. Therefore, this study employed the use of bimetallic (Fe–Co) kaolin-supported catalyst for CNF growth because of high solubility and high rate of diffusion of carbon into the catalyst phase exhibited by Fe–Co as well as strong affinity of raw kaolin to provide a strong base for anchoring these catalysts. In addition, no study is available in literature on the use of response surface methodology (RSM) to study the influence of synthesis parameters (reaction temperature, deposition time, acetylene/hydrogen flow rate and argon flow rate) and their interactions on the yield of CNF grown using kaolin-supported bimetallic catalyst.

Thus, the present study is targeted at preparation of carbon nanofibers onto kaolin-supported Fe–Co catalyst using a wet impregnation method followed by catalytic decomposition of acetylene in a CVD reactor. The prepared bimetallic catalyst and CNFs were characterized for their morphology, microstructures, elemental composition, phase structure, surface area, thermal profiles, and surface oxidation states by HRSEM, HRTEM, EDS, XRD, BET, TGA and XPS.

2 Experimental

2.1 Materials

The kaolin used in this study was obtained from Ejigbo area of Lagos State, Nigeria and used as received without any further treatment. Chemicals such as Co $(NO_3)_2{\cdot}6H_2O$, and $Fe(NO_3)_3{\cdot}9H_2O$, were obtained from Sigma Aldrich, USA, while H_2SO_4 and HNO_3 are obtained from Kem light lab., Mumbai India and Guangdong Guanghua Chemical Factory Co., Ltd, China, respectively. All the chemical used are of analytical grades with percentage purity in the range of 98–99.99%. The carbon source $(C_2H_2)/(H_2)$ and carrier gas (Ar) were supplied by BOC Gases Nigeria Plc, Lagos, Nigeria.

2.2 Methods

2.2.1 Design of experiments (DOE)

A sequential optimization of process variables as controllable inputs for the Fe–Co/kaolin catalyst and CNF production were carried out. The statistical software MINITAB 16 was used to design the experiments and data were analyzed using RSM-based central composite design (CCD) to establish the optimum experimental conditions. All the four variables were coded at two levels corresponding to the upper and lower values of each variable as shown in Table 1. The limits of each variable were inferred from previous work for the development of similar catalysts [29]. The response optimizer of the software was used to determine the desirability of the results.

Table 1 Levels of factors considered in RSM-based CCD in catalysts synthesis procedures

	Drying time (h)	Drying temp. (°C)	Stirring speed (rpm)	Mass of support (g)
Upper (+) level	12	120	400	10
Lower (−) level	8	100	200	8

2.2.2 Synthesis of Fe–Co/kaolin catalyst

The bimetallic catalyst Fe–Co on kaolin support was prepared as described elsewhere [30] by a wet impregnation method, which is targeted mainly at the dispersion of the Fe and Co active components into the pores of the kaolin surface. In this study, 3.62 g and 2.47 g of nitrate salts of iron and cobalt compounds, $Fe(NO_3)_3{\cdot}9H_2O$ and $Co(NO_3)_2{\cdot}6H_2O$, respectively, were weighed and dissolved in 50 mL of distilled water, followed by the addition of a known weight of kaolin under continuous stirring for 30 min. The resulting slurry was allowed to dry at room temperature after which it was oven dried at 120 °C for 12 h, cooled to room temperature, ground and finally screened through a 150-µm sieve. The dried catalyst was ground to avoid agglomeration. This procedure was repeated in accordance with the experimental matrix presented in Table 3 to investigate the influence of drying time, drying temperature, stirring speed and mass of support on the yield of catalyst. The yield of the catalyst after drying was calculated using the relationship presented in the following equation and the result obtained is presented in Table 3:

$$\text{Yield}_{\text{Dried}}\ (\%) = \frac{\text{mass of catalyst after oven-drying}}{\text{initial mass of mixture}} \times 100\% \,. \quad (1)$$

The fine powder (the catalyst) obtained as best yield from Table 3 was calcined by varying the calcination temperature and time using 2^2 factorial design to determine the influence of calcination parameters on the properties especially the yield and the surface area. The yield of the catalyst after calcinations was determined using the following equation and the result is presented in Table 4:

$$\text{Yield}_{\text{Calcined}}\ (\%) = \frac{\text{mass of catalyst after calcination}}{\text{mass fter oven-drying}} \times 100\%. \quad (2)$$

2.2.3 Synthesis of CNF

The synthesis of CNF was carried out by the decomposition of acetylene (C_2H_2) gas in a tubular quartz reactor called CVD. The heating rate, reaction temperature and gas stream rates were electronically controlled in the reactor during the synthesis. 0.5 g of the catalyst (Fe–Co/kaolin) was weighed and stacked into a quartz boat (120 mm × 15 mm) at room temperature, weighed and the boat was set in the middle center of the tube. The furnace was heated at 10 °C/min starting at room temperature while argon gas was allowed to flow over the catalyst at a flow rate of 472 mL/min. Once the set reaction temperature of 550 °C was attained, the argon flow was set to the required flow rate after which carbon source (acetylene and hydrogen gas mixture) was introduced. The introduction of hydrogen in the carbon source

was to prevent the formation of CNT. The reaction was then allowed to proceed until the set reaction time of 40 min was attained, after which the carbon source flow was stopped and the furnace allowed to cool down to room temperature under a continuous flow of argon. The boat was then removed from the reactor and re-weighed to quantify the amount of CNF produced. Percentage of CNFs produced was determined using the following equation [29]:

$$\% \text{ CNFs } = \frac{M_{\text{total}} - M_{\text{catalyst}}}{M_{\text{catalyst}}} \times 100, \tag{3}$$

where M_{total} is the total mass of the final catalyst and CNF produced after CVD reaction process and M_{catalyst} is the initial mess of Fe–Co/kaolin catalyst introduced into the CVD reactor.

This procedure was repeated to investigate the influence of reaction time, reaction temperature, carrier gas (argon) flow rate and carbon source/hydrogen (C_2H_2/H_2) flow rate on the yield of CNF using RSM based on CCD. The levels of factors were varied for optimization parameters by considering the operation limit, shown in Table 2.

Table 2 Levels of factors considered in RSM-based CCD for CNF synthesis

	Time (min)	Temperature. (°C)	Argon flow (mL/min)	Acetylene/hydrogen flow (mL/min)
Upper (+) level	40	600	2360	1416
Lower (−) level	30	550	944	472

Table 3 Experimental matrix and the yield of Fe–Co/kaolin catalyst

Run no.	Drying time (h)	Drying temperature	Stirring speed (rpm)	Mass of support (g)	Experimental yield (%)	Predicted yield (%)
1	8	120	200	8	80.51	82.49
2	12	100	200	8	70.23	83.62
3	8	100	200	8	79.18	83.98
4	10	110	300	9	87.66	78.37
5	12	100	400	10	52.18	63.47
6	12	120	400	8	80.86	81.34
7	12	100	400	8	72.14	70.33
8	8	100	200	10	63.64	76.43
9	8	100	400	8	52.86	66.64
10	12	120	200	10	87.22	86.71
11	8	120	400	10	86.41	86.29
12	8	100	400	10	61.43	66.98
13	10	110	300	9	87.66	78.37
14	12	120	400	10	93.21	88.29
15	12	120	200	8	93.32	87.65
16	12	100	200	10	64.10	68.87
17	8	120	400	8	77.03	72.13
18	10	110	300	8	90.69	78.37
19	10	110	300	9	87.66	78.37
20	8	120	200	10	87.07	88.76
21	10	110	500	9	73.80	74.37
22	6	110	300	9	90.98	81.43
23	10	110	100	9	96.51	90.13
24	10	110	300	7	79.76	82.55
25	10	130	200	9	68.45	93.92
26	14	110	300	9	83.35	83.07
27	10	110	300	9	87.66	82.25
28	14	110	300	9	83.35	70.58
29	10	110	300	9	87.66	82.25
30	10	110	300	11	83.41	81.95

2.2.4 Purification of CNF

In the purification process, 1 g of as-synthesized CNF was weighed and placed inside a 50-mL beaker containing 30 mL of distilled water. 0.1 M HNO_3 and H_2SO_4 mixture (v/v 3:1) was then added to the as-synthesized CNF in the beaker to treat and remove the impurities present. Distilled water was added to make the content up to 100 mL. The mixture was stirred vigorously and then sonicated for 90 min at 40 °C in an ultrasonic bath to introduce oxygen group to the surface of the treated CNFs so as to open the edges for substrate binding. The oxidized CNF was then cooled to room temperature and 300 mL of distilled water was added to wash off the acid. More distilled water was added until the pH became neutral. The slurry was filtered and the residue oven dried at 120 °C for 12 h. The dried CNF was grounded and sonicated to prevent agglomeration and thereafter characterized.

2.2.5 Characterization of Fe–Co/kaolin catalyst and CNF

The as-produced catalyst, as-synthesized and purified CNFs were characterized. Thermogravimetric analysis (TGA 4000, Perkin Elmer, USA) was used to determine the thermal stability. Brunauer–Emmett–Teller (BET; NOVA 4200e, Quantachrome Instruments, USA) was utilized to determine the surface area based on nitrogen adsorption–desorption isotherm. The degree of crystallinity, morphology, elemental compositions and microstructure of the samples were determined using X-ray diffractometer (XRD; PW 1800 diffractometer, Philips, The Netherlands), high-resolution scanning electron microscope coupled with electron diffraction spectrometer (HRSEM-EDX; JEM 100S, JEOL Ltd., Japan), and high-resolution transmission electron microscope (HRTEM, Philips CM20 FEG, The Netherlands). The surface oxidation states of the CNFs were determined using X-ray photoelectron spectroscopy (XPS).

3 Results and discussions

3.1 Effects of catalyst synthesis parameters

Catalyst preparation parameters are the significant factors that controls its quality and quantity and hence its catalytic activities. These factors include drying temperature and time as well as the stirring speed and mass of support used [30–32]. The experimental design matrix employed by RSM and the resulted yield is presented in Table 3.

From Table 3, the optimal yield of 96.51% catalyst was obtained at optimal temperature, time, mass of support and stirring speed of 110 °C, 10 h, 9 g and 100 rpm, respectively. It was obvious that the optimum yield obtained was at a center point between the lower and higher settings for the parameters studied. This is attributed to the fact that when the samples were dried at 100 °C for 12 h, there was a complete loss of bound water. Further increase in temperature to 110 °C and reducing the time to 10 h, though more of evaporation will take place but there is tendency for the condensation of moisture which diffuses into the matrix of the catalyst thus increase in the weight of catalyst occurred and the yield was further enhanced. However, a lowest yield of 52.18% was obtained at drying temperature (100 °C), drying time (12 h), stirring speed (400 rpm) and mass of support (10 g) because the moisture diffusion during impregnation was faster than the solute adsorption on the surface of the kaolin matrix at higher stirring speed (400 rpm), more of the moisture were lost due to evaporation at a prolonged drying time (12 h). These resulted into enhancement of the movement of moisture from the bulk of the catalyst hence the reduction in the mass of the resulting catalyst.

3.2 Temperature and time effect after calcination

The sample obtained at optimum conditions after drying was calcined to study the influence of calcined time and temperature on the yield and surface area of the Fe–Co/kaolin catalyst. The calcination was employed to remove the residual moisture present in the samples and accelerate the conversion of nitrates into their respective oxides. Visual observation revealed that all the samples turned darkish brown after calcination due to the complete removal of moisture. The result of the 2^2 factorial design of the four samples obtained after calcination is presented in Table 4.

From Table 4, it could be observed that an optimum yield 78.73% was obtained after calcinations at 500 °C for 14 h and the yield of catalyst decrease with increase in temperature. This could be attributed to the complete transformation of metal salts to metallic oxides. It could also mean that high temperature caused partial transformation of highly dispersed iron oxide nanocrystallite into fayalite normally found in silica walls that is embedded in kaolin support [31]. This result is in line with the work of Abdulkareem et al. [30] and Nukleonika [33] who reported

Table 4 Factorial experimental matrix showing yield and surface area after calcination

Samples	Calcination temperature (°C)	Calcination time (h)	Yield (%)	Surface area (m^2/g)
B	500	14	78.73	318.670
C	500	16	73.64	190.836
D	600	14	71.49	376.477
E	600	16	70.15	306.828

the same observation. Thus, increase in calcination time from 14 to 16 h was responsible for the reduction in the yield due to destruction of the hollow structures in the precursor. In addition, the table revealed that increase in calcination time from 14 to 16 h, at a temperature of 500 °C, the surface area decreased from 318.670 to 190.836 m^2/g. The same observation occurred at 600 °C (from 376.477 to 306.828 m^2/g). This could be attributed to more moisture lost at higher temperatures due to evaporation as well as structural change due to dehydroxylation of the supported material (kaolin) during calcination at higher temperature as reported by Francisca [34]. However, all the samples have higher surface area enough to be used as catalyst for synthesis of CNF in a CVD reactor because according to Bawa et al. [35], all the materials having a surface area value above 100 m^2/g are considered having a high surface area and are a potential material to be employed as catalyst.

3.3 Kaolin characterization results

Prior to synthesis of catalyst, the raw kaolin sample received from Ejigbo Lagos state, Nigeria was characterized to monitor the changes in physical, chemical and microstructural properties to determine its suitability as catalyst support for CNF growth in a CVD reactor.

3.3.1 Surface area

The surface area of raw kaolin sample was determined using BET and the result showed that there was no significant change in the surface area of raw kaolin (106.2 m^2/g) and the dried catalyst (99.8 m^2/g). This could be due to the fact that at pre-calcination, the catalyst was only dried to remove moisture and as a result, the drying temperature was not enough to result in significant change in the surface area due to evaporation. Other possible reason could be due to the blockage of kaolin pores by the catalyst and vice versa. On the other hand, the surface area of the catalyst increases from 99.8 to about 376.5 m^2/g after calcinations due to structural change in kaolin due to dehydroxylation. This same observation was reported by Francisca [34]. The author's report showed that during dehydroxylation of kaolin, change in structure that took place resulted in expanded layers of silicates in form of montmorillonites, smectites and other vermiculites which were not removed during heat treatment, hence contributed to increase in surface area. Bawa et al. [35] reported that porous materials with surface area greater than 100 m^2/g are a potential material for catalyst support. Thus, the value obtained for kaolin is slightly higher than that reported by Bawa and colleagues; this validates the choice of kaolin as a support material.

3.3.2 XRD analysis of kaolin

The phase identification and the crystallinity of the kaolin sample were carried out using XRD. The result of the analysis is shown in Fig. 1.

The results as presented in Fig. 1 shows ten diffraction peaks at 2θ value of 8.9°, 12.4°, 19.9°, 24.9°, 26.6°, 28.0°, 35.0°, 38.3°, 50.1° and 62.2° with corresponding crystal plane of (001), (110), (210), (220), (221), (321), (400), (411), (521) and (542). The presence of mica and quartz at 2θ value of 8.9°, 24.9°, 38.3° and 50.1° was as a result of silicate minerals present in the kaolin sample. The XRD study confirmed that the resultant kaolinite are mixture of simple cubic, body-centered cubic and combinations of face-centered cubic. The average lattice parameters from indexing of the peaks in the XRD were calculated to be 9.9882 Å. The particle diameter of the kaolin sample was calculated using the Debye–Sherrer equation:

$$D = \frac{0.9\lambda}{\beta \cos\theta}, \tag{4}$$

where λ is the wavelength of the X-ray (0.1541 nm), β is the full width at half maximum (FWHM), θ is the diffraction angle in radian, and D is the particle diameter size. The interspacing between the atoms (d) was calculated using the Bragg's law given as:

$$d = \frac{\lambda}{2\sin\theta}. \tag{5}$$

Using Eqs. 4 and 5, lattice parameters (a) were calculated and the results are presented in Table 5.

From Table 5, the average interspacing between the atoms, average crystal size and average lattice parameters of the kaolin sample are 0.3764 nm, 17.480 nm and 10.03 Å, respectively. These indicated that the kaolin sample used shows characteristic that is of less interplanar spacing which support reflections at higher orders. This wider angle between the unit cell of the kaolin crystal of 10.03 A is more than the reported values of a well-crystallized kaolinites

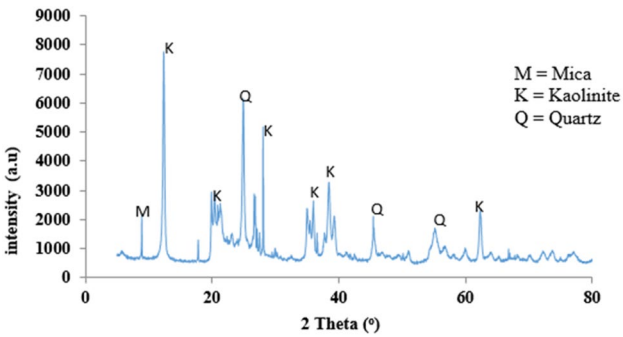

Fig. 1 XRD spectra of kaolin sample

Table 5 Indexing results for kaolin characterization

Peak no.	2θ	β (nm)	D (nm)	D (nm)	a (Å)
1.	8.9	0.0962	0.9926	8.182	9.93
2.	12.4	0.0824	0.7135	9.964	10.09
3.	19.9	0.0824	0.4458	10.058	9.97
4.	24.9	0.0549	0.3574	14.203	10.11
5.	26.8	0.0549	0.3324	14.257	9.97
6.	28.0	0.0823	0.3184	10.209	10.07
7.	35.0	0.0274	0.2559	29.085	10.25
8.	38.5	0.0275	0.2337	29.706	9.92
9.	45.5	0.0543	0.1992	16.710	9.96
10.	62.4	0.0275	0.1487	32.429	9.98

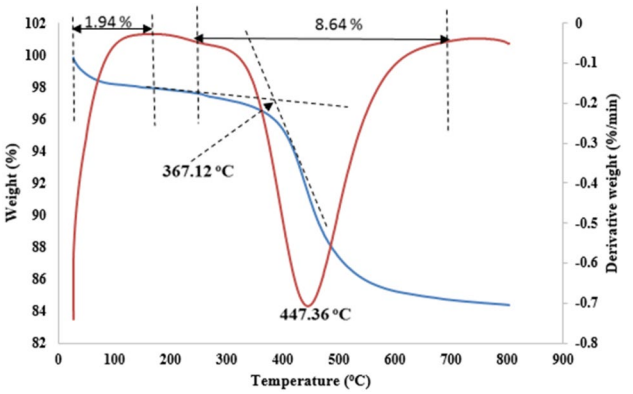

Fig. 2 TGA/DTA curve of kaolin

having a graphitic line of 001 d-spacing of 7.1–7.2. The difference could be connected with a small amount of interlayer water within the kaolin crystals. However, there are some incompleteness and imperfections in some patterns in Fig. 1 indicating the overshadowing amounts of other minerals of clay size with the kaolin. Some peaks related to crystallized phase were also detected, which is attributed to quartz and mica initially present in the kaolin. The kaolin showed well-defined diffraction angles at 2θ values of 12.4° and 19.9° corresponding to the d crystal particle size of 9.964 nm and 10.058 nm with corresponding crystal plane of (100) and (110), respectively. This is a little bit different from that obtained by Sachin et al. [36] who reported the typical characteristic peaks of kaolinite at 2θ value of 12 and 25. The difference may be due to the presence of pristine phase of mica and quartz in the sample not detected at the diffraction angle of less than 12.4. However, the graphitic line of this sample observed at 12.4 and 19.9 may be as a result of low contents of quartz and mica impurities present in the sample at 2θ values of 24 and 31 as reported by [37].

3.3.3 Thermogravimetric and differential thermal analysis of kaolin

The thermal stability of the kaolin sample was also investigated and the result is shown in Fig. 2.

The TGA curve shown in Fig. 2 revealed three weight lost regimes. The first occurred between the temperatures of 26.75–180.06 °C which corresponds to weight loss of about 1.94%. This represents the loss of hygroscopic water. Second, the conversion of kaolin sample into kaolinite started at the onset temperature at 367.12 °C. However, the conversion was due to the presence of some impurities such as quartz and mica as shown in Fig. 2. This result is in close agreement with the report of Kovo [38] and Shani et al. [39]. Third, the main weight loss occurred at the peak temperature of 447.36 °C with a corresponding weight loss of 12.61%. Weight loss at this temperature may be linked to dehydroxilation process of the kaolin sample when the structural OH component of kaolin is lost in form of water. This is in line with the work of Francisca [34] who reported the same observation. The transformation of kaolin into kaolinite due to heat treatment is presented in the following equation:

$$2Al_2Si_2O_7(OH)_4 \rightarrow 2Al_2Si_2O_7 + 2H_2O. \quad (6)$$

The TGA curve also showed that the kaolin sample is stable up to temperature above 600 °C which implies that the kaolin could be used as a support for catalyst synthesis.

3.4 Statistical analysis of Fe–Co/kaolin catalyst

Statistical analysis was carried out for the purpose of studying the influence of synthesis parameters on the yield of Fe–Co/kaolin catalyst using MINITAB 16 software. Analysis of variance (ANOVA) was used to generate the statistical model for the mean and combined effects of these process parameters on the yield of catalyst and the result is presented in Table 6.

The estimated model for the yield (Y) as a function of all the four factors was obtained and is presented in the following equation:

$$\begin{aligned}\text{Yield } (\%) = {} & -308.677 + 6.6A + 5.71B - 0.34C \\ & + 16.67D - 0.37AA - 0.04BB - 2.87DD \\ & + 0.07AB + 0.01AC - 0.9AD + 0.01BC \\ & + 0.35BD + 0.02CD,\end{aligned} \quad (7)$$

where A = drying time, B = drying temperature, C = stirring speed and D = mass of support.

One important observation in the regression model is that there is main and interaction effects between the factors considered. It can be generally deduced from the main effects of the model that increase in drying time, drying temperature, and mass of support which increase the yield and hence

Table 6 (ANOVA) for the yield of Fe–Co/kaolin catalyst

Source	*F* value	*P* value	Remark
Regression	1.48	0.235	
Linear	2.72	0.073	
A	0.04	0.850	
B	7.44	0.016	Significant
C	3.39	0.087	
D	0.00	0.946	
Square	1.56	0.238	
A^2	0.54	0.473	
B^2	4.60	0.050	Significant
C^2	0.98	0.339	
D^2	2.06	0.173	
Interaction	0.61	0.721	
AB	0.28	0.607	
AC	0.15	0.705	
AD	0.47	0.503	
BC	0.44	0.516	
BD	1.74	0.209	
CD	0.57	0.464	
Residual error		0.000	
Lack of fit	89.02		

have positive effect on the yield. This is in line with the result obtained from Table 3 which showed that the optimum yield of catalyst was obtained when there was a increase in drying temperature from 100 to 110 °C, drying time from 8 to 10 h and mass of support from 8 to 9 g. However, the stirring speed has negative effect on the yield, implying that low setting of stirring speed (100 rpm) leads to an optimum yield of the catalyst as shown in Table 3.

The results of the *P* value and *F* test values as presented in Table 6 showed that the model was not significant with a *P* value of 0.235 and *F* value of 1.48. However, only the temperature variable of the linear part of the model is significant with a *P* value of 0.016 and *F* value of 7.44 corresponding to about 98.4% confidence level at α value of 0.05. This same observation occurred for the squared part of the model with a *P* value of 0.05 and *F* value of 4.60 corresponding to 95% confidence level at the same α value. This observation suggests that the effect of temperature on the yield of catalyst is independent of other variables. The interaction part of the model was also not significant with a *P* value of 0.721 and *F* value of 0.61. The non-significance ability of some parameters might be attributed to the choice of confidence level. Consequently, the only significant factor (drying temperature) was analyzed and a reduced model which contains the factor was generated. The reduced desirable model is shown as follows:

$$\text{Yield } (\%) = -308.270 + 5.71B - 0.04B^2. \quad (8)$$

3.5 Characterization results for Fe–Co/kaolin catalyst

3.5.1 HRSEM analysis of Fe–Co/kaolin catalyst

The surface morphology and the elemental composition of the produced catalyst before and after calcination were carried out using HRSEM/EDX and the results are presented in Fig. 3.

The HRSEM images of the pre-calcined catalyst depicted in Fig. 3a showed a plate-like nature of psuedohexagonal flexible sheets of kaolin crystals with irregular particle shapes. The structure might be related to the strong interaction bond in aluminosilicate materials, the dominant component of kaolin [34, 40, 41] used as a support during impregnation. It was also observed that the catalyst components of the sample agglomerates with some amorphous impurities as the drying temperature of 120 °C was not enough to disperse and reduce the Fe–Co catalyst components into their respective nanoparticles [12, 42]. The EDX spectrum revealed different percentage compositions of the following elements: Fe, Co, Al, Si, C and O.

Figure 3b–e show the micrographs of HRSEM image of the catalyst after calcination at different temperatures and drying time. From the figures, it could be seen that the particles irrespective of the calcination temperature contains micro pores. This is an indication that the pores allow for dispersion of the iron and cobalt nanoparticles into the matrix of the kaolin. The dispersion of Fe–Co nanoparticles on the kaolin support is also evidenced in the accompanied EDX spectrum which revealed the presence of Fe, Co, C, O, Al and Si in the sample. There is evidence of agglomerations in the sample with mixture of shapes ranging from hexagonal to spinel. Meanwhile, as the calcination temperature increases, the shape of the particles turned nearly spherical with reductions in agglomerates due to heat treatment during calcination stage. This might be as a result of large surface provided by the kaolin support. Researchers such as Mahmoud et al. [43], Liluia et al. [44] and Honarbakhsh et al. [45] reported that in calcination, temperature of iron–cobalt catalyst was responsible for the occurrence increase or agglomeration and the morphological changes to sphere-like shape. The observe changes might be attributed to the formation of some intermediates such as spinel Fe_2O_3 in form of hematite as well as Co_3O_4 and $CoFe_2O_4$ [43]. The lumps of active catalyst formed during calcination process further support its suitability for the growth of CNF. From Fig. 3b, it could be observed that at 500 °C, drying time of 14 h, the Fe–Co/kaolin particles are closely packed unlike stack with loosely bound ends observed at 600 °C for 14 h. However, when the drying time of the calcined catalyst was increased to 16 h irrespective of the temperature, it was

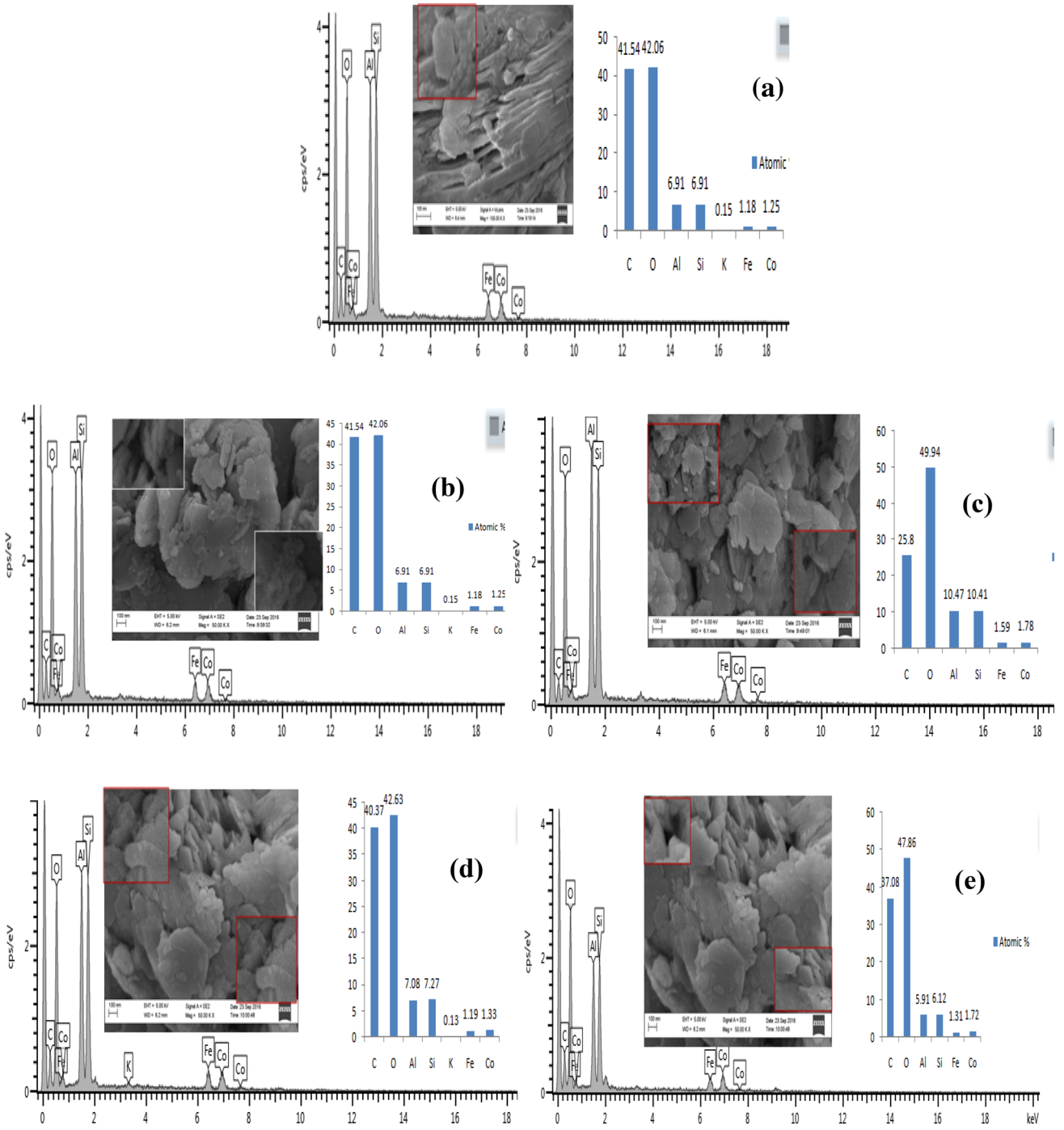

Fig. 3 HRSEM/EDX image of Fe–Co/kaolin catalyst sample **a** after drying, **b** after calcinations at **a** 500 °C/14 h, **c** after calcination at 600 °C/14 h, **d** after calcination at 500 °C/16 h and **e** after calcination at 600 °C/16 h

observed that the morphological arrangement of the Fe-Co/kaolin particles was similar.

The accompanied EDX results from the figures also showed that at the calcination temperatures of 500 °C and 600 °C, all the samples contain Fe and Co in ratio 1:1 by mass as used in catalyst preparation. In addition, the ratio of the percentage composition of elements in kaolin support used in this study (Al:Si:O ≃ 1:1:3) was not in close agreement with what is obtained for kaolin (Al:Si:O ≃ 1:1:6). This might be as a result of dehydroxylation of kaolin as well as reduction of iron and cobalt salt into their respective oxides ($CoFe_2O_4$, Fe_2O_3, and Co_3O_4) during calcination.

3.5.2 XRD analysis of Fe–Co/kaolin catalyst

The phase identification and formation of the catalyst was studied by XRD and the result is presented in Fig. 4.

According to Fig. 4, a high intense peak was observed at 2θ value of 26.42° with crystal plane of (220) attributed to quartz (SiO_2) in the kaolin support formed via dehydroxylation during heat treatment. The peak was pronounced because of its unreactive nature. The peak at 2θ value of 20.69° and 35.30° with crystal plane (111) and (311) are assigned to $CoFe_2O_4$ while other peak such as 49.9° with crystal plane (400) is attributed to CoO_3 and Fe_2O_3 [43, 45]. Several other peaks in the pre-calcination catalysts suggest that the drying temperature of 120 °C was not enough to reduce the iron and cobalt salts into their respective oxides. On the other hand, some of these peaks disappeared upon calcination of samples at higher temperatures of 500 and 600 °C. The calcined samples showed the diffraction peaks at 2θ values of 20.69°, 26.42°, 35.30°, 49.9° and 60.10° with corresponding crystal planes of 111, 220, 311, 400 and 422, all of which revealed the formation of cobalt ferrite with a face cubic structure (FCC) [45]. The figure also shows that as calcination temperature increases, there is no significant change in the peaks as well as their intensity. The crystal particle size of the samples at pre-calcination was 32.6 nm, but upon calcination at higher temperature of 500 °C, the average crystallite size reduces to 31.8 nm and 28.0 nm at 14 and 16 h, respectively. The same reduction in average crystallite size was observed upon calcination at temperature of 600 °C (14 h, 27.3 nm; 16 h, 27.9 nm). The reduction in crystallite size might be attributed to attrition of particles as a result of heat treatment.

3.6 Synthesis and optimization of CNF

The versatility of CVD method used for mass production of CNF to meet its increasing demand necessitated optimization of its synthesis parameters. RSM was used to design an experiment to determine and optimize the influence of the synthesis parameters such as reaction temperature, reaction time, flow rate of argon and flow rate of acetylene/hydrogen ratio on the yield of CNF. The experimental matrix and the result of the yield obtained are presented in Table 7.

From the result presented in Table 7, it was noticed that highest yield of 348% CNF was obtained at a reaction temperature of 600 °C, reaction time of 40 min, argon flow rate of 1416 mL/min and acetylene/hydrogen flow rate of 1416 mL/min. The higher percentage yield observed was as a result of enough residence time of 40 min that allowed the production and growth of CNF, at a reaction temperature of 600 °C. In addition, low flow rate of hydrogen in the feed promoted the reduction of oxygen content in the reaction zone by expanding the clustered bond in the carbon molecule, hence more acetylene flow and growth was enhanced. However, low yield of 16% was noticed at the following process conditions: reaction temperature (600 °C), deposition time (30 min), argon flow rate (2360 mL/min) and acetylene/hydrogen flow rate (944 mL/min). This suggests that low residence time of 30 min had led to suppression of CNF growth because the amount of carbon source fed into the reactor was also low and promoted agglomeration of the catalyst hence reduction of rate of decomposition of acetylene to carbon.

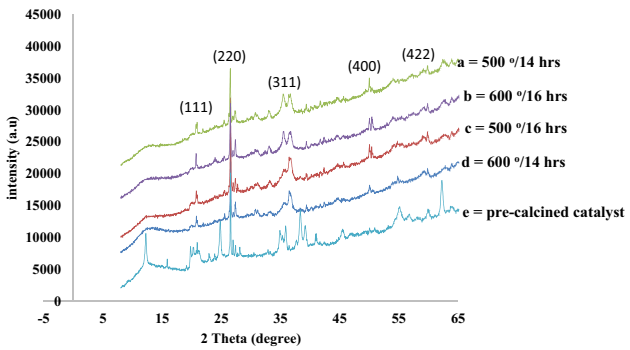

Fig. 4 XRD spectra of Fe–Co/kaolin catalyst

3.6.1 Effect of reaction temperature

The growth of CNF in a CVD reactor is governed by the heat treatment needed for the decomposition of the precursor gas (acetylene), the diffusion of the carbon formed onto the matrix of the support and subsequent deposition of the carbon in form of CNF Amogh et al. [46]. In view of this, the influence of reaction temperatures between 525 and 625 °C on the yield of CNF was carried out and the result showed that an increase in reaction temperature from 550 to 600 °C lead to increase in the yield of CNF from 108 to 348% at constant acetylene/hydrogen flow rate ratio of 2. This suggests the existence of linear relationship between the reaction temperature and the yield as a result of rapid decomposition of acetylene which produces more carbon. Beyond 600 °C, at the same acetylene/hydrogen flow rate ratio, a slight decrease in the yield of CNF was observed, which could be ascribed to the lost of more acetylene in the reaction environment as a result of dehydroxylation of supported catalyst used. This result is in line with the findings of Ali et al. [21], Antonio et al. [47] and Rinaldia et al. [48]. The authors opined that increase in temperature increase the yield of CNF due to faster decomposition of acetylene at higher temperature.

Table 7 The yield of CNF from RSM-based CCD matrix

Run no.	Temperature (°C)	Time (min)	Argon flow (mL/min)	Acetylene/hydrogen flow (mL/min)	Experimental yield (%)	Predicted yield (%)
1	550	40	1416	944	108	98
2	600	30	1416	944	214	211
3	550	30	1416	944	120	147
4	575	35	1888	1180	136	136
5	600	30	2360	1416	214	179
6	600	40	2360	944	68	100
7	600	30	2360	944	16	61
8	550	30	1416	1416	234	158
9	550	30	2360	944	66	69
10	600	40	1416	1416	348	300
11	550	40	2360	1416	283	242
12	550	30	2360	1416	194	163
13	575	35	1888	1180	136	136
14	600	40	2360	1416	296	289
15	600	40	1416	944	142	193
16	600	30	1416	1416	256	247
17	550	40	2360	944	48	77
18	575	35	1888	1180	136	136
19	575	35	1888	1180	136	136
20	550	40	1416	1416	206	180
21	575	35	2832	1180	124	114
22	525	35	1888	1180	136	186
23	575	35	944	1180	167	202
24	575	35	1888	708	120	20
25	575	45	1888	1180	192	189
26	625	35	1888	1180	324	298
27	575	35	1888	1180	136	136
28	575	25	1888	1180	100	128
29	575	35	1888	1180	136	136
30	575	35	1888	1652	96	220

3.6.2 Effect of acetylene/hydrogen flow rate

The role played by hydrogen in the synthesis of CNF is very important. This is because the presence of hydrogen CNF growth serves as reducing agent to oxygen content in the reaction environment not only to promote the synthesis quality. This happened via stoppage of clustered dangling bond at the edges of the graphitic CNF to prevent the formation of tubular graphene shells. However, by controlling the relative amount of hydrogen in the gas phase, it is possible to change the structure of carbon formation from tube to fibers. This study, therefore, investigates the effect of acetylene/hydrogen flow ratio on the yield of CNF. The optimum temperature of 600 °C was chosen while varying the acetylene/hydrogen flow rate ratio between 1 and 3 at 0.5 intervals. The result as presented in Table 7 revealed that at acetylene/hydrogen flow rate ratio of 1, the yield of CNF was 120%, however, decreased to 68% upon increase in the flow ratio to 1.5, showing that the hydrogen in the feed had suppressed the formation of carbon available for reaction withdrawing little acetylene supplied for reaction. When hydrogen supply is of equal amount with the main carbon source such as acetylene, there is tendency for the suppression of production of CNF due to low residence time as a result of high-velocity profile created by high relative hydrogen flow rate to acetylene [12]. Yehya et al. [5] also reported that hydrogen presence in the mixture of the carbon source in synthesis of CNF could serve as a blocking agent inhibiting the active sites for conversion. However, as the flow ratio increases to 2.5, the yield increases to 348%. This result could be attributed to the release of excess acetylene for easy conversion to carbon. However, further increase in flow ratio of hydrogen to acetylene lead to decrease in yield of CNF. This happened because at flow ratio of 3, carbon available for reaction has been exhausted.

3.6.3 Effect of reaction time

Another process parameter that played major role in the CNF growth is reaction time. Though, CNF can be synthesized within few minutes of reaction, but at a prolonged residence time, the surface area, and morphology could be altered [5]. By careful control of these process parameters, the desired CNF can be produced in large quantity [47]. This paper reports the effect of reaction time from 25 to 45 min on the yield of CNF at constant temperature of 600 °C, acetylene/hydrogen flow rate ratio of 2.5 and constant argon flow rate and the result obtained depicted that as the reaction time is increased from 30 to 40 min, there was a decrease in yield from 256 to 136%, and then increase to 348% at 40 min, thus the CNF yield fluctuated. The increase in the yield of CNF with an increase in time may be connected to decrease in rate of diffusion of carbon into the matrix of the catalyst at increased temperature until the carbon supply into the system was exhausted hence decrease in yield. The increase in the yield observed at higher deposition time could be attributed to the rate of decomposition of acetylene due to high catalytic activity of the Fe–Co particles as a result of high diffusion of carbon into the matrix of the catalyst via active site generated by the kaolin support. This result is in line with the findings of Mustafa et al. [49] who reported the same observation.

3.6.4 Effect of argon flow rate

For the synthesis of CNF in a CVD reactor, an inert gas which acts as a carrier gas is needed to purge the system of air thereby preventing oxidation of carbon. Most widely used carrier gases are argon and nitrogen though sometimes hydrogen is employed to reduce the oxygen contents of the reaction environment. For the desired CNF amount, the flow rate of inert gas (argon in this study) was controlled and studied to evaluate its effect on the yield of CNFs. This was done by varying argon flow rate from 944 to 2832 mL/min, keeping other parameters constant. It could be observed from Table 7 also that increasing the argon flow rate from 944 to 1416 mL/min, there was an increase in the yield of CNF. This result is attributed to lower rate of transfer of acetylene molecule from the catalyst surface. However, as the flow rate of argon was further increased to 2360 mL/min, a corresponding decrease in the yield of CNF was noticed because the rate at which carbon moved out of the reacting surface has increased thereby disallowing high deposition of carbon on the surface of the catalyst. These results are in agreement with the work of Aliyu et al. [18] and Idowu [50] who independently found that increase in flow rate of argon implied increase in the rate of carbonaceous materials as a result of coverage and number of acetylene molecules on the catalyst metal nanoparticle's surface. In addition, there was another transit decrease in CNF yield noticed at an increased argon flow rate from 1416 to 1888 mL/min. This showed that argon as a carrier gas has the tendency of either suppressing or improving the decomposition rate of acetylene [18, 42].

3.7 Statistical analysis of CNF synthesis

Statistical optimization of the process parameters was carried out to determine the correlation between the experimental and simulated results. Minitab's Response Optimizer was used to calculate individual desirability using utility transfer function. This was done by selecting weight (from 0.1 to 10) to determine how much close is the experimental to the optimized values and the result is shown in Table 8.

From Table 8, composite desirability of 1 was observed suggesting that the settings connote favorable results for the responses as a whole. Be that as it may, the individual desirability shows that the settings are more effective at maximizing yield (0.98077) than at minimizing reaction temperature, reaction time, acetylene/hydrogen flow rate and argon flow rate.

The correlation between the experimental and predicted yield was determined from the plots of the experimental and predicted yield data. The result presented in Fig. 5 indicates that they fall within both statistical and experimental acceptability ($R^2 = 0.7333$) with optimal solution obtained

Table 8 Solutions of the optimized and experimental yield

Operating parameters	Optimized solution	Experimental solution
Reaction temperature (°C)	625	600
Reaction time (min)	45	40
Acetylene/hydrogen flow rate ratio (mL/min)	2.5	2.5
Argon flow rate (mL/min)	2832	1416
Desirability	1.000	

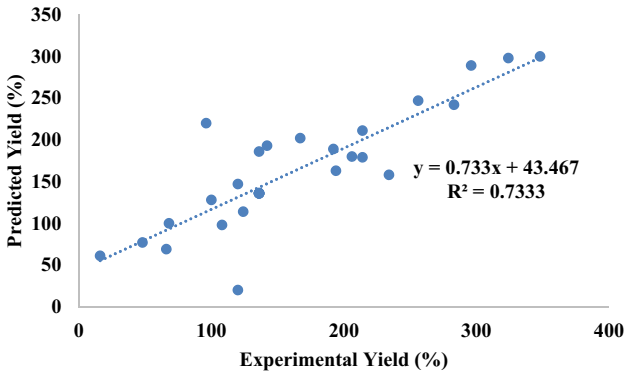

Fig. 5 Plots of experimental and predicted yield of CNF

at reaction temperature of 625 °C, reaction time of 45 min, acetylene/hydrogen flow rate ratio of 2.5 and argon flow rate of 2832 mL/min.

The interactive effects of the process variables were carried out using analysis of variance (ANOVA), a three-dimensional response surface and two-dimensional contour plots. This was done to test the significance and accuracy of the model generated from the designed experiment using Minitab 16 software. The result is presented in Table 9.

The estimated model for the yield (Y) as a function of all the four factors was obtained and is presented in the following equation:

$$\begin{aligned}\text{Yield}\ (\%) = {} & 136 + 55.92A + 30.75B - 44.08C \\ & + 100D + 106.29AA + 22.29\,BB \\ & + 21.79CC - 15.71DD + 30.75AB \\ & - 72.25AC + 24.75AD + 56.25BC \\ & + 82.25CD,\end{aligned} \tag{9}$$

where A represents the reaction temperature; B represents reaction time; C represents argon flow rate and D represents acetylene/hydrogen flow rate.

One important observation in the regression model has to do with the main and interaction effects between the factors considered. It can be generally noticed from the main effects of the model that reaction temperature, reaction time and acetylene/hydrogen flow rate increase the yield hence exerted positive effects while argon flow rate has negative effect due to decreased yield of the CNF synthesized.

Table 9 ANOVA results on significant factors of the process parameters on the yield of CNF

Source	F value	P value	Remark
Regression	2.93	0.024	Significant
Linear	7.08	0.002	Significant
A	5.53	0.033	Significant
B	1.67	0.216	
C	3.43	0.084	
D	17.70	0.001	Significant
Square	1.58	0.232	
AA	5.70	0.031	Significant
BB	0.25	0.624	
CC	0.24	0.631	
DD	0.12	0.729	
Interaction	1.07	0.423	
AB	0.28	0.605	
AC	1.54	0.234	
AD	0.18	0.677	
BC	0.93	0.350	
BD	1.50	0.240	
CD	1.99	0.178	

This result is in close agreement with the results obtained in Table 7 which showed that highest yield of CNF was obtained when the CVD reactor was operated at higher levels of reaction temperature, reaction time and acetylene/hydrogen flow rate and at a lower level of argon flow rate. The interaction effects from the model showed that there were significant interactions among the studied variables on the response (yield).

The P and F values were used to check the significance of the tested variables and their interactions. The results of the P value and F test values presented in Table 9 revealed the significance of the model, its linear part, drying temperature as well as acetylene/hydrogen flow rates having P values of 0.024, 0.002, 0.033 and 0.001 with corresponding F values of 2.93, 7.08, 5.53 and 17.70, respectively. These correspond to 97.6, 99.8, 96.7 and 99.9% confidence level at an α value of 0.05. This same observation occurred for the temperature of the squared part of the model with a P value of 0.031 and F value of 5.70 corresponding to 96.9% confidence level at the same α value. These observations suggest that the effect of temperature and acetylene/hydrogen flow rate is independent of other variables. The interaction part of the model was not significant with a P value of 0.423 and F value of 1.07. The non-significance ability of some parameters might be attributed to the choice of confidence level [18, 40]. Consequently, the two significant factors, reaction temperature and acetylene/hydrogen flow rate, were analyzed and a reduced model which contains the two factors were generated. The reduced desirable model is shown by the following equation:

$$\begin{aligned}\text{Yield}\ (\%) = {} & 147.02 + 55.92A + 100.08D \\ & + 100.78AA - 21.22DD + 24.75\,AD.\end{aligned} \tag{10}$$

Though, some of the tested variables were found to be statistically non-significant, their effects and their interactions were shown to be practically significant from the experiments. The significance of these variables was determined using the contour and surface plots and the result is presented in Fig. 6.

From Fig. 6a, b, it can be noticed that a simple maximum contour plots were obtained while the surface plot represents a falling ridge which implies that at constant argon flowrate and acetylene/hydrogen flow of 1888 mL/min and 1.5 where curvature was obtained, respectively, yielded more than 350% CNF when the CVD was operated at a temperature of above 620 °C for more than 40 min. These are factor settings above the prescribed in the experiment and depicted that operating at that level could maximize the yield of CNF. However, this is in contrast with the experimental result presented in Table 7, where optimum yield of about 348% was obtained. The possible reason for this was that the experimental reaction had earlier occurred at 35 min before it was discovered that more carbon generated

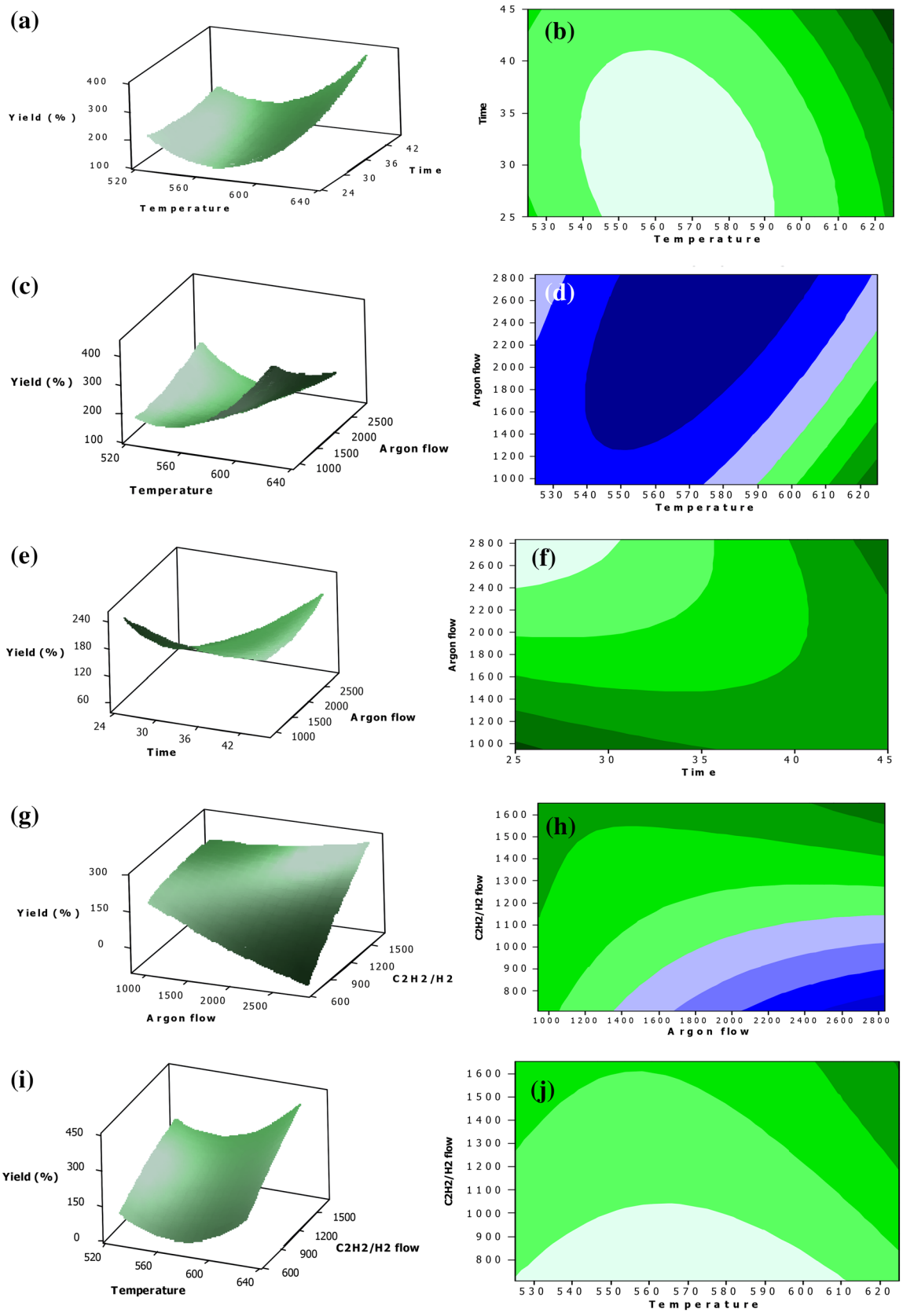

Fig. 6 Surface and contour plots of effect of **a**, **b** reaction time and temperature; **c**, **d** argon flow and temperature; **e**, **f** argon flow and time; **g**, **h** argon flow and acetylene/hydrogen flow; **i**, **j** temperature and acetylene/hydrogen flow on the yield of CNF

from the decomposition of acetylene was still held at the surface of the catalyst due to low residence time. The falling ridge surface and rising ridge contour plots as presented in Fig. 6c, d demonstrated the effect of temperature and argon flow rate on CNF yield. From the figure, it could be observed that to maximize the yield of CNF, the reaction temperature need to be increased from 600 °C to above 620 °C, while argon flow rate need to be increased from around 1100 to less than 1500 mL/min. This implies that a combination of high-level temperature and low-level argon flow rate could lead to more yield of CNF. This might be attributed to lower rate of transfer of carbon molecule from the catalyst surface, even though the operating temperature is enough for complete decomposition of acetylene. The effect of combination of time and argon flow rate on the yield of CNF is presented in Fig. 6e, f. It is obvious from the figure that to maximize CNF yield, argon flow rate of about 2500 mL/min is needed at a minimum time of about 25 min. This implies that at higher argon flow rate, the tendency for mass transport of carbon from the surface of the catalyst could be reduced if the reaction takes place at a shorter time. The surface and contour plot of Fig. 6g, h represent the effect of combinations of argon flow rate and acetylene/hydrogen flow rate on CNF yield. The figure shows that maximum yield of CNF could be obtained by maximizing both argon flow rate and acetylene/hydrogen flow rate ratio. This might be associated with the fact that as more argon flows into the system, more acetylene is needed to compensate for the loss of carbon from the catalyst surface. A combination of higher temperature and high acetylene/hydrogen flow favored high yield of CNF (Fig. 6i, j).

3.8 Characterization results of CNF

3.8.1 Morphological arrangement and size distribution

The morphology and size distribution of as-synthesized and purified CNF were examined using HRSEM while the internal texture diameter and size distributions were measured by a HRTEM. The HRSEM and HRTEM images of as-synthesized and purified CNF are presented in Fig. 7.

From Fig. 7a, b, it could be observed that the as-synthesized sample contain CNFs in a winding form surrounded by impurities from kaolin used as catalyst support. The micrograph also contains spread of Fe–Co catalyst nanoparticles which was used to promote the growth of CNF in the CVD reactor. After acid treatment, the sample contains twisted form of CNF with homogenous size entangled cover one another and grow both in length and diameter as observed in Fig. 7b. Though, impurities in form of amorphous carbon, metal catalyst as well as the support materials were still noticed in the purified catalyst, substantial parts of them were removed as evidenced in the EDX spectrum of the purified sample. Complete removal of the impurities cannot be achieved as this often lead to destruction of the fiber structure.

The result of HRTEM revealed from Fig. 7c that the nanofibers have inner diameter in the range of 19.5–40 nm. The outer diameter of CNF ranges between 25 and 100 nm which could be controlled by adjusting the synthesis time [51].The image also showed that the diameter of purified CNF remain the same with as-synthesized CNF, an indication that there was no significant change brought about by the influence of acid treatment. Some metal particles were maintained at both the middle and the end of the fibers showing that the growth process might follow the deposition diffusion–nucleation growth mechanism [52]. The formation of metal particles at the middle of the fibers indicated that the support material (kaolin) had provided numerous active sites in which nucleation and subsequent growth of CNFs were obtained because of the presence of many metal oxides. This observation is in contrast with tip or base growth mechanism observed with the use of other support materials such as alumina, silica, and calcium carbonates [53]. However, during purification, it was observed that some deformations were formed on the fibers (see Fig. 7d). These deformations exhibited are one of the disadvantages of using acid treatments method for purification of CNF.

3.8.2 Elemental composition and thermal stability

Figure 8a, b presents the EDX spectrum and elemental composition of both as-synthesized and purified CNF while Fig. 8c depicted the thermal stability of both as-synthesized and purified CNF as determined by TGA.

Figure 8a showed the presence of elements such as C, O, Fe, Si, Al and Co were present with atomic composition of 71.14, 18.99, 0.11, 5.53, 4.07 and 0.13% in the as-synthesized CNF, respectively. The presence of these elements could be traced to catalyst used in the production of CNF. In purified spectrum shown in Fig. 8b, there is presence of C, O, Si and Fe. The presence of Fe and Si might be associated with their incomplete removal during acid treatment process. However, it is worth of notice that the percentage composition of CNF in as-synthesized sample increased from 71.14 to 98.61% after purification. This showed that the purification process improves the composition of CNF as other impurities such as Fe, and Si were significantly removed.

The thermal profile of as-synthesized and purified CNFs as shown by Fig. 8c indicated that there was a rapid initial mass loss between the temperatures of 64.48–122.03 °C for as-synthesized CNF (A-CNF). This initial mass loss could be attributed to the presence of impurities in form of amorphous carbon and some associated defective sites which were not thoroughly initiated during growth in the CVD reactor. These defective sites were improved with

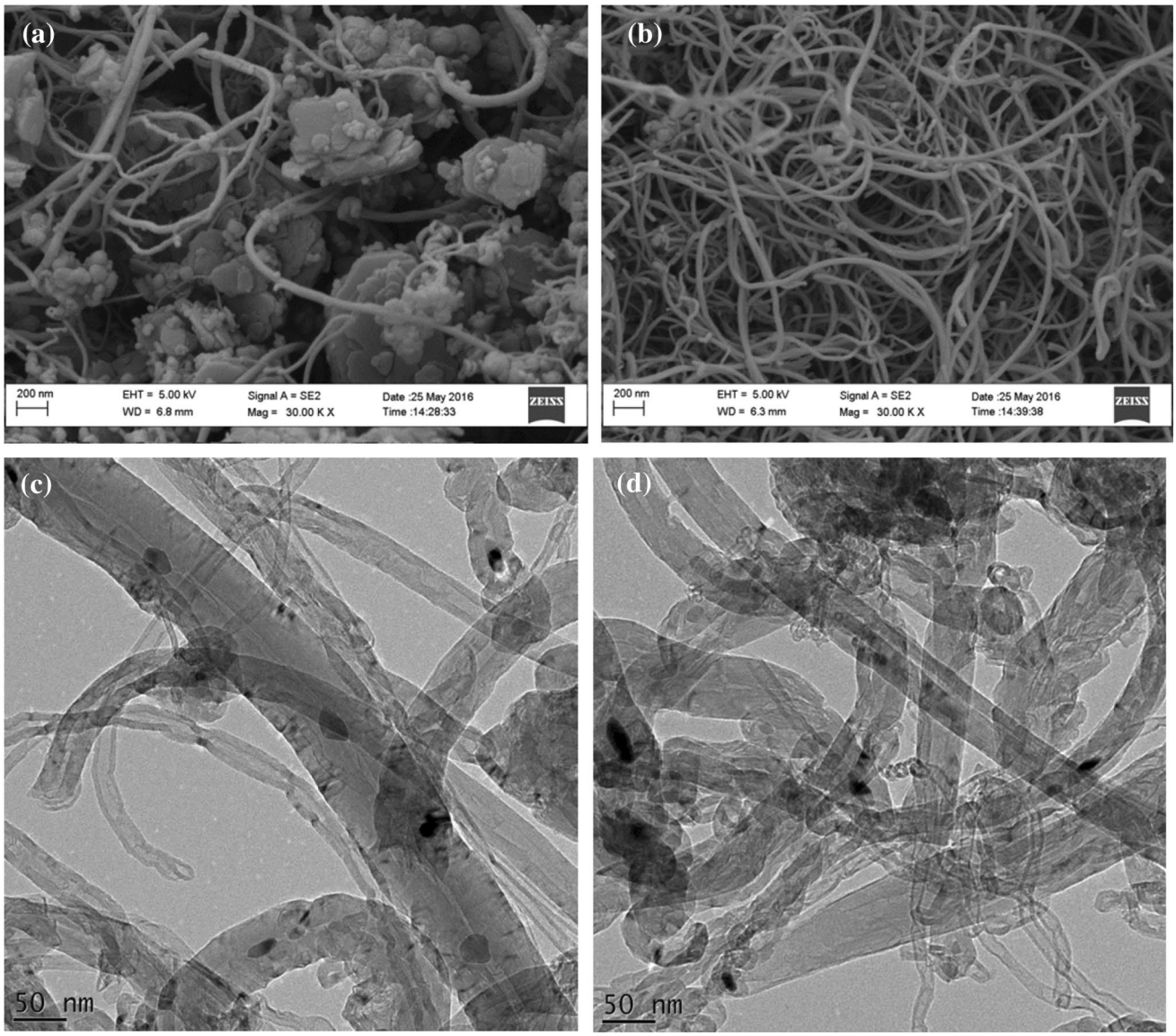

Fig. 7 HRSEM image of **a** as-synthesized CNF and **b** purified CNF, **c** HRTEM image of as-synthesized CNF showing the internal and external fiber diameter, **d** HRTEM image of purified CNF showing the deformation as a result of acid treatment

the acid treatment using combination of H_2SO_4 and HNO_3, with the purified CNF (P-CNF) showing a constant pattern within these ranges of temperatures, although, some volatile components were lost. The decomposition of the purified CNF starts at a temperature of 209.75 °C and terminated at a temperature of 433.21 °C showing a mass loss of about 88%. This shows that the purified CNF is relatively pure. The 12% impurities might be due to the presence of metallic particles which were trapped within the pores of the CNF and could not be removed by acid treatment. However, the as-synthesized CNF curve indicated a decomposition initiation at a temperature of about 196.77 °C with its residual mass at the temperature of about 389.53 °C representing mass loss of about 69%. This attributes could be linked to the presence of some traces of kaolinites as impurities which were embedded in the sample. The TGA profile of purified CNF as presented showed that the P-CNF is stable up to a temperature of about 433.21 °C implying that it could be applied for further applications.

3.8.3 XRD analysis of CNF

The phase structure of as-synthesized and purified CNFs was examined using XRD and the result is shown in Fig. 9.

According to Fig. 9, two major diffraction peaks at 2θ value of 26.31° and 44.32° are noticed for as-synthesized CNF while in the case of purified CNFs, a slight decrease in 2θ values earlier noticed for as-synthesized CNFs

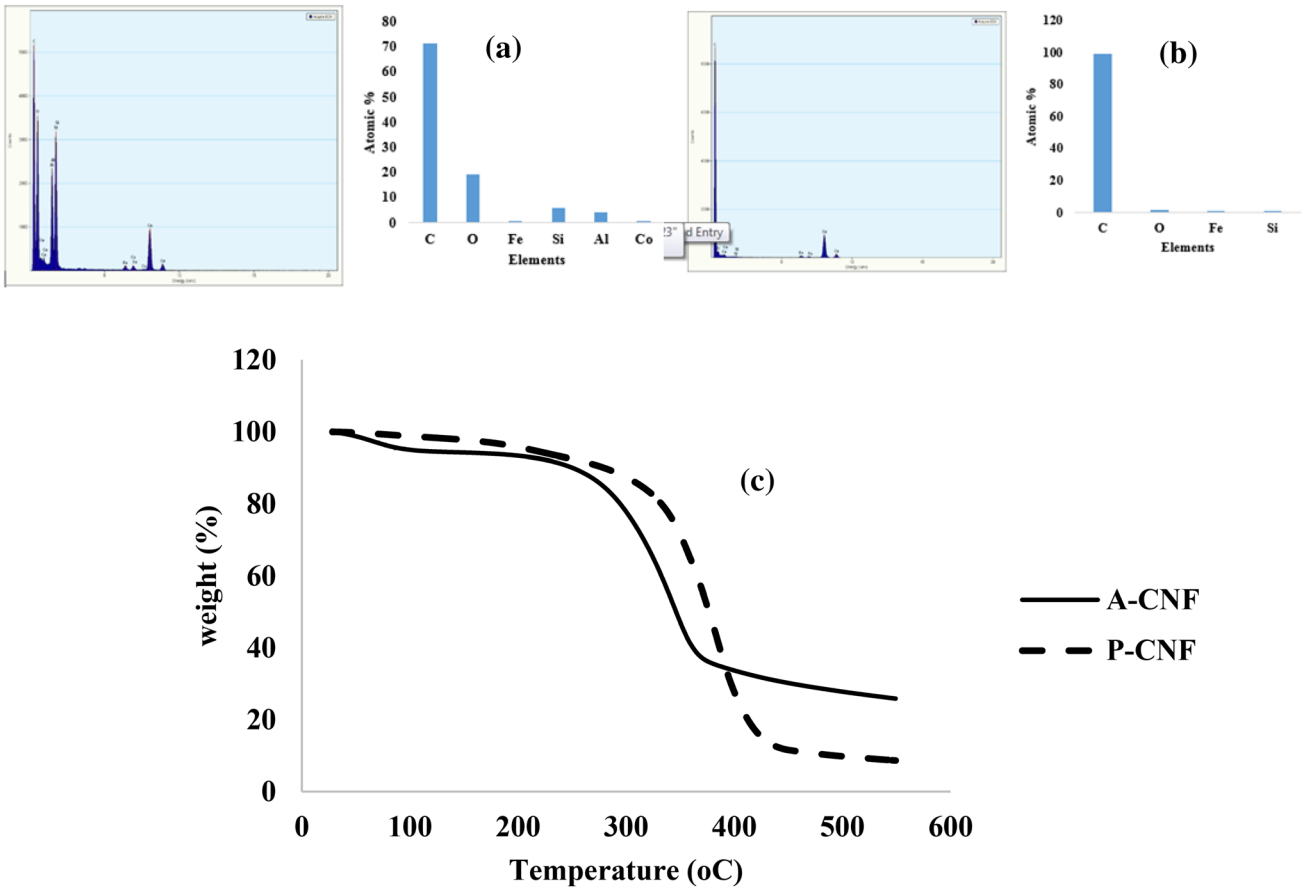

Fig. 8 EDX spectrum of **a** as-synthesized CNF, **b** purified CNF showing their elemental compositions, **c** thermal stability of CNF

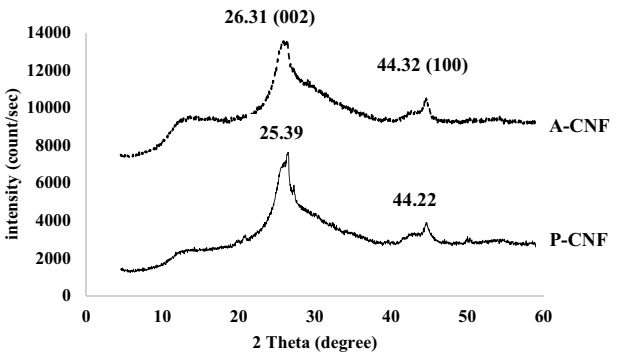

Fig. 9 XRD spectrum of A-CNF and P-CNF

specifically was found to be 25.39° and 44.22°. The slight difference might be associated with the process of purification. All these major peaks are in line with the identified peaks for carbon in hexagonal-graphitized form [3, 12, 54]. However, the peaks observed for P-CNFs were in form of graphitized carbon and high crystallinity than A-CNFs as evidenced in their sharpness. The figure also showed that the different peaks correspond to the crystal plane of (002) and (100) with corresponding d-spacing of 0.3354 nm and 0.3451 nm, respectively. The d-spacing is as a result of interlayer of graphites and further support the fact that the crystals in the carbon phase are well packed and arranged in orderly manner.

3.8.4 X-ray photoelectron spectroscopy (XPS) analysis of CNF

The surface oxidation of the elements formed on both A-CNF and P-CNF was determined using XPS and the result is presented in Fig. 10.

The general XPS survey of A-CNF as presented in Fig. 10a revealed the presence of C, O, Si, and Ar. The presence of carbon and oxygen was due to the carbon source (acetylene) and air used during synthesis and growth of CNF in a CVD reactor. Argon (Ar) presence was due to Ar beam utilized during sputtering. The major components such as the C (1s) and O (1s) occurred at binding energy of 284.6 eV and 535.5 eV, respectively, while the small contamination of Si (2p) present at 105.5 eV binding energy originated

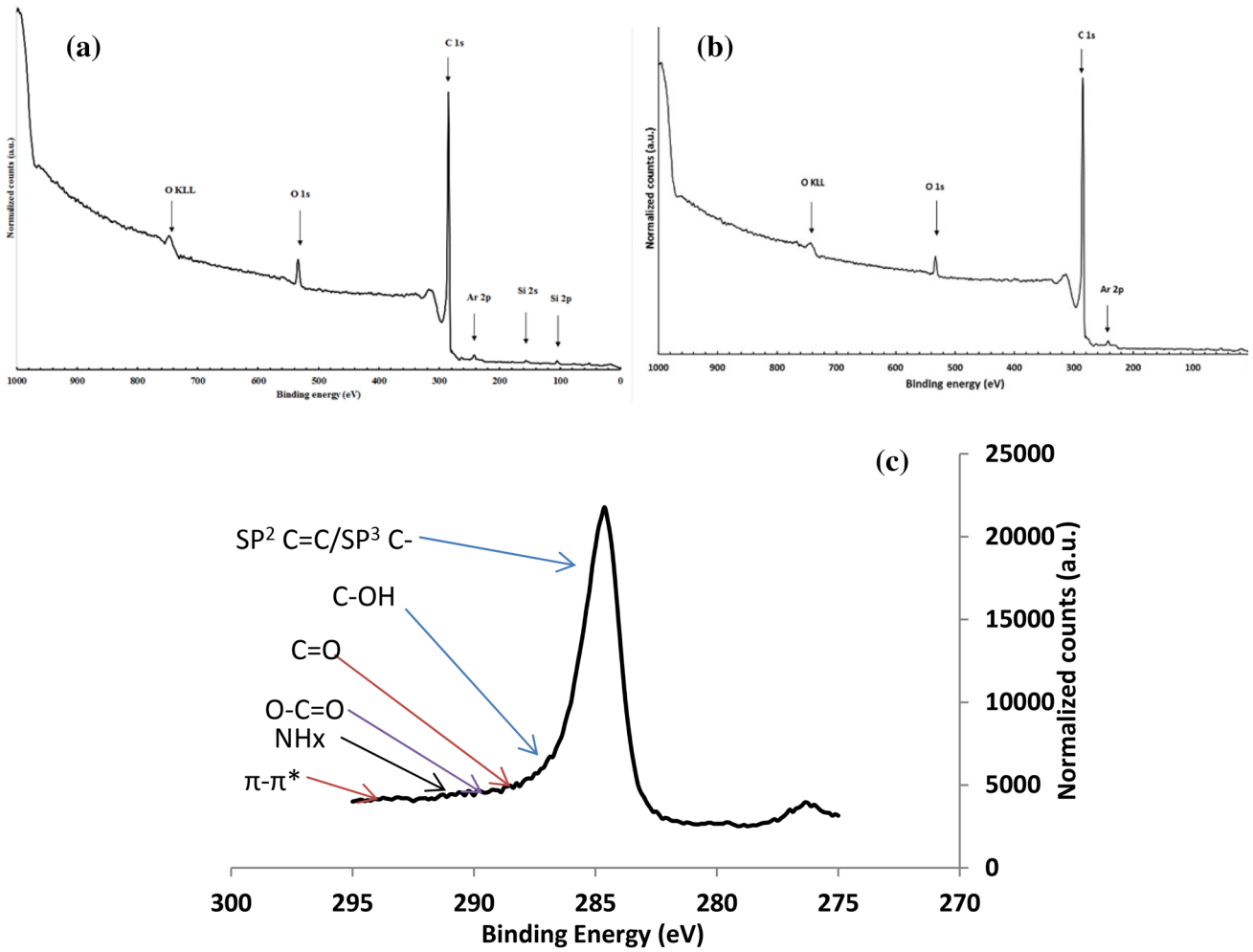

Fig. 10 wide scan spectrum of **a** A-CNF, **b** P-CNF, **c** deconvoluted spectrum of C 1s

from the kaolin support used for the synthesis of catalyst. Reported observations of [51] showed that the binding energy of silicon as a reinforcing material was between 103 and 105 eV. Higher binding energy obtained in this study was as a result of local charging and that the silicon presence serves as impurities but not as composite. Non-detection of Fe and Co suggested that the two metals are encapsulated within the inner pores of the CNFs.

The sputtered envelope of the XPS analysis result of purified CNF (P-CNF) is presented in Fig. 10b. After purification of CNF, its anchoring sites were opened allowing the addition of some functional groups hence oxidation occurred. The result as presented in the figure shows that the counts of C (1s) (binding energy of 284.56 eV) and oxidized O (1s) (binding energy of 534.5 eV) was obvious revealing that all other impurities in form of nanoparticles have been removed during purification. The HRTEM micrograph further shows that Fe and Co were encapsulated within the matrix of the CNFs due to their non-detection by the XPS. It was also noticed that Si (2p or 2s) was not found on the surface of the P-CNF, suggesting that the Si was trapped within the wall of the P-CNF.

Figure 10c revealed the presence of six peaks at their respective binding energies. The main peak (SP^2 C=C/SP^3 C–C) is attributed to the graphitic structure of carbon. Other peaks correspond to hydroxyl functional group (C–OH), attachment of carbonyl (C=O), carboxyl (O–C=O) and nitrate (NHx) groups of the CNF structure. However, the π–π* peak is the transition loss peak, which denote the chemical force of attraction on the surface of the CNFs. This result confirms the work of Jing-Hong et al. [55] and Yaru [56] who independently submitted that deconvolution of carbon peak especially for oxidized carbon produced chemical shift in binding energies of the component elements and that functionality characteristics such as the carbonyl, hydroxyl, and carboxyl group which are exposed created sites for effective adsorption of substrates.

The summary of the C 1s fits for all the specimens and the percentage contribution of each species to the envelope was calculated for both A-CNF and P-CNF and the results are shown in Tables 10 and 11.

The results as presented in the tables showed that both A-CNF and P-CNF contain some oxygen surface groups. The presence of these oxygen-containing groups in A-CNF was due to the formation of carbon dioxides at higher temperature during the growth of CNF in a CVD reactor. P-CNF also contains these oxygen-containing groups probably due to the acid treatment with combination of H_2SO_4/HNO_3 and the percentage of the oxygen-containing compounds was found to increase from (14–20%), (6–8%), (2–3%), (0–1%) for C–OH, C=O, O–C=O and π–π*groups, respectively. This result is supported by the findings of Tijmen et al. [57] who found that carbon nanomaterials treated with H_2SO_4/HNO_3 mixture resulted into increase in oxygen-containing compounds due to the binding effects of the oxygen to the carbon layers at the surface. It was also revealed from the tables that the bindings of elements in terms of the % concentration and area covered for A-CNF are C–C and C=C 74% (12,194), C–OH 14% (2232), C=O 6.0% (1059), O–C=O 4.0% (604), NHx 2.0% (308) and π–π* 0% (76), respectively. While that of P-CNF are C–C and C=C 63.0% (34,724), C–OH 20% (10,853), C=O 8.0% (4638), O–C=O 4.0% (2361), NHx 3.0% (1859) and π–π* 1% (606), respectively These show that purification of CNF with acid treatment has really increased the oxygen-containing functional groups at the surface of the CNF, thereby enhancing its active sites for further applications.

Table 10 C 1s fits result for A-CNF

Binding energy (eV)	Binding energy change	FWHM	Area	Atomic % concentration	Chemical bonds
284.8		1.67	12,194	74	C–C, C=C
286.2	−1.4	1.6	2232	14	C–OH
287.7	−2.9	1.6	1059	6	C=O
289.4	−4.6	1.6	604	4	O–C=O
290.8	−6	1.6	308	2	NH_X
292.3	−7.5	1.5	76	0	π–π*
Total			16,473	100	

Table 11 C 1s fits result for P-CNF

Binding energy (eV)	Binding energy change	FWHM	Area	Atomic % concentration	Chemical bonds
284.54		1.18	34,724	63	C–C, C=C
285.94	−1.4	1.6	10,853	20	C–OH
287.44	−2.9	1.6	4638	8	C=O
289.14	−4.6	1.6	2361	4	O–C=O
290.54	−6	1.6	1859	3	NH_X
292	−7.46	1.6	606	1	π–π*
Total			55,041	100	

4 Conclusion

Model predicting the yield of Fe–Co/kaolin catalyst was developed using RSM. The model was analyzed and found to be sufficient for predicting the effects of the catalyst preparation parameters on the yield with drying temperature showing independent significance to the model. The surface and contour plots of the yield as a function of bi-factors of the model showed positive interactive effects. The results of characterization of the produced catalyst showed that the catalyst possess characteristics that made it suitable for the growth of CNF. The CNF preparation parameters such as the reaction temperature, reaction time, argon flow rate and acetylene/hydrogen flow rate have been shown to have effect on the yield of the CNF. The ANOVA study from the generated data using RSM showed that all the tested parameters are significant either alone or based on the bi-factor relationship as exhibited by the surface and contour plots. The result of HRSEM showed a twisted form of CNF, with a relative diameter of about 19.5 and 40 nm as revealed by HRTEM. TGA result showed that the CNF is thermally stable, XRD result revealed a highly crystalline graphitized CNF, while the XPS showed that the grown CNF contains some surface functional groups capable of enhancing its active sites for further applications.

Acknowledgements This is to acknowledge and appreciate the support received from the Tertiary Education Trust Fund (TETFUND) of Nigeria under Grant number TETFUND/FUTMINNA/2017/09. The authors also thank The Centre for Genetic Engineering and Biotechnology (CGEB) FUTMinna who offered us direct access to their facilities. We are also grateful to the following people that helped analyze the samples: Dr. Remy Bucher, (iThemba Labs), Cape Town, South Africa for XRD; Dr. Franscious Cummings, Electron Microscope Unit (EMU), Physics Department, University of Western Cape (UWC), South Africa for HRTEM; Adrian Joseph, Physics department, UWC, South Africa for HRSEM and Prof. W. D. Roos, Physics Department, University of the Free State, South Africa for XPS.

Compliance with ethical standards

Conflict of interest The authors reported no potential conflict of interest relevant to this study

References

1. Krijn P, De J, John W (2000) Carbon nanofibers: catalytic synthesis and applications. Catal Reform Sci Eng J 42:4
2. Feng L, Xie N, Zhong J (2014) Carbon nanofibers and their composites: a review of synthesizing, properties and applications. Mater J. https://doi.org/10.3390/ma7053919
3. Eun-Sil P, Jong-Won K, Chang-Seop L (2014) Synthesis and characterization of carbon nanofibers on Co and Cu catalysts by chemical vapor deposition. Bull Korean Chem Soc 35:6. https://doi.org/10.5012/bkcs.2014.35.6.1687
4. Navaporn K, Surawut C, Takashi S (2016) Control of physical properties of carbon nanofibers obtained from coaxial electrospinning of PMMA and PAN with adjustable inner/outer nozzle ends. Nanoscale Res Lett 11:186. https://doi.org/10.1186/s11671-016-1416-7
5. Yehya MA, Abdullah A, Ahmad TJ, Ma'anFahmi RA (2016) Synthesis and characterization of carbon nanofibers grown on powdered activated carbon. J Nanotechnol. https://doi.org/10.1155/2016/1538602
6. Al-Saleh MH, Sundararaj UA (2009) Review of vapor grown carbon nanofiber/polymer conductive composites. Carbon J. https://doi.org/10.1016/j.carbon.2008.09.039
7. Tawfik AS (2015) Carbon-based nanomaterials for desulfurization: classification, preparation, and evaluation. Adv Chem Mater Eng Book Ser (ACME). https://doi.org/10.4018/978-1-4666-9545-0.ch005
8. Teo KBK, Singh C, Chhowalla M, Milne WI (2003) Catalytic synthesis of carbon nanotubes and nanofibers. In: Nalwa HS (ed) Encyclopedia of nanoscience and nanotechnology. American Scientific Publishers, Stevenson Ranch, pp 665–686
9. Couteau E, Hernadi K, Seo JW, Thien-Nga L, Miko C, Gaal R, Forro L (2003) CVD synthesis of high-purity multiwalled carbon nanotubes using $CaCO_3$ catalyst support for large-scale production. Chem Phys Lett 378:9
10. Kazunori K, Kozo S (2005) Modeling CVD synthesis of carbon nanotubes: nanoparticle formation from ferrocene. Carbon J 43:252–257
11. Ding Q, Xueyin S, Xiujuan Y, Xiaosi Q, Chak-Tong A, Wei Z, Youwei D (2013) Large-scale and controllable synthesis of metal-free nitrogen-doped carbon nanofibers and nanocoils over water-soluble Na_2CO_3. Nanoscale Res Lett 8:545
12. Afolabi AS (2009) Development of platinum electro catalytic electrodes for proton exchange membrane fuel cell. Ph.D. thesis, University of the Witwatersrand, Johannesburg, South Africa
13. László G, Goran B, Erno K (2010) Bimetallic cobalt based catalysts catalysis. Rev Sci Eng 52:133–203
14. Manafi SA, Badiee SH (2007) Production of carbon nanofibers using a CVD method with lithium fluoride as a supported cobalt catalyst. Res Lett Mater Sci. https://doi.org/10.1155/2008/850975
15. Lim S, Shimizu A, Yoon S-H, Korai Y, Mochida I (2004) High yield preparation of tubular carbon nanofibers over supported Co–Mo catalysts. Carbon 42(7):1279–1283. https://doi.org/10.1016/j.carbon.2004.01.027
16. van der Lee MK, van Dillen AJ, Geus JW et al (2006) Catalytic growth of macroscopic carbon nanofiber bodies with high bulk density and high mechanical strength. Carbon J 44:629–637
17. Eunyi J, Heai-Ku P, Jong-Ha C et al (2015) Synthesis and characterization of carbon nanofibers grown on Ni and Mo catalysts by chemical vapor deposition. Bull Korean Chem Soc 36:1452–1459
18. Aliyu A (2016) Synthesis and characterization of carbon nanotubes via novel support in catalytic chemical vapour deposition method. M.Eng. thesis, Federal University of Technology, Minna, Nigeria
19. Mamun AA, Ahmed YM, Muyibi SA, Al-Khatib MFR, Jameel AT, AlSaadi MA (2016) Synthesis of carbon nanofibers on impregnated powdered activated carbon as cheap substrate. Arab J Chem. https://doi.org/10.1016/j.arabjc.2013.09.001
20. Prasantha RM, Larisa IN, Albert GN, Andrzej C, Markus V, Karin H, Jari EM, Maarit JK, Vesa P, Tatiana SK, Oleg VT, Esko IK (2009) Synthesis of carbon nanotubes and nanofibers on silica and cement matrix materials. J Nanomater. https://doi.org/10.1155/2009/526128
21. Ali S, Muthana M, Ahmad D (2015) Synthesis of carbon nanofibers from decomposition of liquid organic waste from chemical and petrochemical industries. Int Conf Technol Mater Renew Energy Environ Sustain 74:4–14
22. Sang-Suk K, Ki-Won K, Hyo-Jun A, Kwon-Koo C (2008) Characterization of graphitic nanofibers synthesized by the CVD method using nickel–copper as a catalyst. J Alloys Compd 449:274–278
23. Qian D, Xueyin S, Xiujuan Y, Xiaosi Q, Chak-Tong A, Wei Z, Youwei D (2013) Large-scale and controllable synthesis of metal-free nitrogen-doped carbon nanofibers and nanocoils over water-soluble Na_2CO_3. Nanoscale Res Lett 8:545
24. Junfeng G, Ian AK, Charanjeet S, Vladimir BG, Brian FGJ, Milo SP, Syali L, Alan HW (2005) Production of carbon nanofibers in high yields using a sodium chloride support. J Phys Chem B. https://doi.org/10.1021/jp051544w
25. Benjamín VS, Nicolás DS, Nicola N, Mario CA, José M, Bastidas R, Roumen Z, Margarita S (2017) Synthesis of carbon nanofibers with maghemite via a modified sol–gel technique. J Nanomater. https://doi.org/10.1155/2017/5794312
26. Roman MK, Yuri IB, Alexander MV, Ilya VM, Aleksey AV (2018) Synthesis of carbon nanofibers by catalytic CVD of chlorobenzene over bulk nickel alloy. Russ Fed Appl Surf Sci. https://doi.org/10.1016/j.apsusc.2017.08.227
27. Jian-Ying M, Hwang DW, Narasimhulu KV, Lin P-I, Yit-Tsong C, Sheng-Hsien L, Lian-Pin H (2004) Synthesis and properties of carbon nanospheres grown by CVD using kaolin supported transition metal catalysts. Carbon J 42:813
28. Zong-Xiang X, Jing-Dong L, Roy VAL, Yan O, Dai-Wei L (2005) Catalytic synthesis of carbon nanotubes and carbon spheres using kaolin supported catalyst. Mater Sci Eng J B 123:102–106
29. Aliyu A, Kovo AS, Abdulkareem AS et al (2017) Synthesize multi-walled carbon nanotubes via catalytic chemical vapour deposition method on Fe–Ni bimetallic catalyst supported on kaolin. Carbon Lett. https://doi.org/10.5714/CL.2017.21.033
30. Abdulkareem AS, Suleiman B, Abdulazeez AT et al (2016) Factorial design of optimization of monometallic cobalt catalyst on calcium carbonates support for carbon nanotube synthesis. In: Proceedings of the World congress on engineering and computer science, San Francisco, USA
31. Hu M, Peiling D, Zhang Y, Gao J, Ren X (2016) Effect of reaction temperature on carbon yield and morphology of CNTs on copper loaded nickel nanoparticles. J Nanomater 2016:1–5
32. Mhlanga SD, Mondal KC, Carter R et al (2009) The effect of synthesis parameters on the catalytic synthesis of multiwalled carbon nanotubes using Fe–Co/$CaCO_3$ catalysts. S Afr J Chem 62:67–76
33. Surowiec Z, Wiertel M, Budzyński M, Gac W (2013) Synthesis and characterization of iron-cobalt nanoparticles embedded in mesoporous silica MCM-41. Nukleonika 58:87–92
34. Francisca UN (2014) Application of zeolite 4a—metakaolin matrix for the removal of some heavy metals from crude oil tank farm wastewater. Ph.D. thesis, Ahmadu Bello University, Zaria
35. Bawa SG, Ahmed AS, Okonkwo PC (2016) The study of thermal effect on the surface properties of gamma-alumina synthesized from Kankara Kaolin. Niger J Technol 35:1

36. Kumar S, Panda AK, Singh RK (2013) Preparation and characterization of acids and alkali treated kaolin clay. Bull Chem React Eng Catal 8:1
37. Diko ML, Ekosse GE (2013) Characterisation of two kaolin facies from Ediki, Southwest Cameroon. Acad J 8:18. https://doi.org/10.5897/sre12.577 **(ISSN 1992-2248)**
38. Kovo AS (2011) Development of zeolites and zeolite membranes from Ahoko Nigerian Kaolin. Ph.D. thesis, The University of Manchester, Manchester, UK
39. Shani S, Paolo R, Nigel M, Kate W (2011) Dehydroxylation of kaolinite to metakaolin—a molecular dynamics study. J Mater Chem. https://doi.org/10.1039/c0jm01748e
40. Lenka V, Eva P, Silvie V, Ivan K (2011) Characterization and differentiation of kaolinites from selected Czech deposits using infrared spectroscopy and differential thermal analysis. Acta Geodyn 8:59–67
41. Aroke UO, El-Nafaty UA, Osha OA (2013) Properties and characterization of kaolin clay from Alkaleri, North-Eastern Nigeria. Int J Emerg Technol Adv Eng 3:11. https://www.researchgate.net/…/281378945
42. Alhassan MI (2016) Formulation of bimetallic (Fe–Co) catalyst on $CaCO_3$ support for carbon nanotube synthesis. M.Eng. thesis, Federal University of Technology, Minna, Nigeria
43. Mahmoud GN, Elias BS, Hossein AA, Abdul HS, Mansor H (2010) Simple synthesis and characterization of cobalt ferrite nanoparticles by a thermal treatment method. J Nanomater. https://doi.org/10.1155/2010/907686
44. Lilia A, Najeh ML, Bessaïs V, Madigou S, Villain S, Leroux C (2014) Magnetic, electric and thermal properties of cobalt ferrite nanoparticles. Mater Res Bull. https://doi.org/10.1016/j.materresbull.2014.06.029
45. Honarbakhsh S, Farahmandjou M, Behroozinia S (2016) synthesis and characterization of iron cobalt (FeCo) nanorods prepared by simple co-precipitation method. J Fundam Appl Sci 8:892–900
46. Amogh NK, Virginia AD, Bruce JT (2012) Carbon nanofiber synthesis within 3-dimensional sintered nickel microfibrous matrices: optimization of synthesis conditions. J Nanotechnol. https://doi.org/10.1155/2012/396269
47. Antonio L, Agustı G, Paula S, Amaya R, Jose LV (2005) Growth of carbon nanofibers from Ni/Y zeolite based catalysts: effects of Ni introduction method, reaction temperature, and reaction gas composition. Ind Eng Chem Res. https://doi.org/10.1021/ie05
48. Rinaldia A, Abdullaha N, Ali M et al (2009) Controlling the yield and structure of CNF grown on a nickel/activated carbon catalyst. Carbon 47:3023–3033
49. Mustafa M, Mohammed AA, Rasel D et al (2018) Optimization of the synthesis of superhydrophobic carbon nanomaterials by chemical vapor deposition. Sci Rep. https://doi.org/10.1038/s41598-018-21051-3
50. Idowu AO (2016) Development of a suitable bimetallic (Fe–Co) catalyst on kaolin support for carbon nanotube synthesis. M.Eng. thesis, Federal University of Technology, Minna, Nigeria
51. Chang-Seop L, Yura H (2016) Preparation and characterization of CNF and its composites by chemical vapor deposition. Open Book Publication, Cambridge
52. Zhanbing H, Jean-Luc M, Aurélien G, Chang SL, Didier P, Costel SC (2011) Iron catalysts for the growth of carbon nanofibers: Fe, Fe_3C or both? Chem Mater 23:5379–5387. 10.1021/cm202315j|
53. Wei X (2006) Synthesis, characterization and catalytic application of carbon- and silica-based nanocomposites. Ph.D. dissertation, Ruhr-University Bochum, Hebei, China
54. Kim YI, Soundararajan D, Park CW et al (2009) Electrocatalytic properties of carbon nanofiber web-supported nanocrystalline Pt catalyst as applied to direct methanol fuel cell. Int J Electrochem Sci 4:1548–1559
55. Jing-Hong Z, Zhi-Jun S, Jun Z, Ping L, De C, Ying-Chun D, Wei-Kang Y (2007) Characterization of surface oxygen complexes on carbon nanofibers by TPD, XPS and FT-IR. Carbon J. https://doi.org/10.1016/j.carbon.2006.11.019
56. Yaru N (2012) Surface silanization of CNF and nanotubes for altering the properties of epoxy composites. PhD Thesis, Ilmenau University of Technology, Thuringia, pp 32–33
57. Tijmen GR, Adrianus JD, John WG, Diederik CK (2002) Surface oxidation of carbon nanofibres. Chem Eur J 8:5. https://doi.org/10.1002/1521-3765(20020301)8:5%3C1151:AID-CHEM1151%3E3.0.CO;2-%23